Mineralogical Magazine, 2014, Vol. 78(2), pp. 447–465

Mössbauerite, $Fe^{3+}_6O_4(OH)_8[CO_3]\cdot 3H_2O$, the fully oxidized 'green rust' mineral from Mont Saint-Michel Bay, France

J.-M. R. GÉNIN[1,*], S. J. MILLS[2,*], A. G. CHRISTY[3], O. GUÉRIN[4], A. J. HERBILLON[5], E. KUZMANN[6], G. ONA-NGUEMA[7], C. RUBY[1] AND C. UPADHYAY[8]

[1] Institut Jean Barriol FR2843 Université de Lorraine-CNRS, ESSTIN, 2 rue Jean Lamour, F-54500, Vandœuvre-Lès-Nancy, France
[2] Geosciences, Museum Victoria, GPO Box 666, Melbourne 3001, Victoria, Australia
[3] Centre for Advanced Microscopy, Sullivans Creek Road, Australian National University, Canberra 0200, ACT, Australia
[4] Laboratoire de Géomorphologie, École Pratique des Hautes Études, 15 boulevard de la mer, F-35800 Dinard, France
[5] Unité des Sciences du Sol, Université Catholique de Louvain, B-1348 Louvain-la-Neuve, Belgium
[6] Department of Chemistry, Eötvös Lorand University, Pazmany Peter setany, H1117, Budapest, Hungary
[7] Institut Minéralogie et de Physique, Milieux Condensés, Université Pierre et Marie Curie, F75252 Paris, France
[8] School of Materials Science & Technology, IT-Banaras Hindu University, 221005 Varanasi, India

[*Received 19 September 2013; Accepted 14 March 2014; Associate Editor: G.D. Gatta*]

ABSTRACT

The new mineral mössbauerite (IMA2012–049), $Fe^{3+}_6O_4(OH)_8[CO_3]\cdot 3H_2O$, is a member of the fougèrite group of the hydrotalcite supergroup. Thus, it has a layered double hydroxide-type structure, in which brucite-like layers $[Fe^{3+}_6O_4(OH)_8]^{2+}$ are intercalated with CO_3^{2-} anions and water molecules. Mössbauerite is the fully oxidized analogue of fougèrite and trébeurdenite, related to them chemically by the exchange of $(Fe^{3+}O^{2-})$ with $(Fe^{2+}OH^-)$. Mössbauerite, intimately intergrown with trébeurdenite, was discovered in intertidal gleys from Mont Saint-Michel Bay, France, along with quartz, feldspars and clay minerals. Mössbauerite is formed by the oxidation of the other members of the fougèrite group. Like them, it occurs as µm-scale platelets in gleys with restricted access to atmospheric O and decomposes rapidly when exposed to air. Identification and characterization of these minerals has relied on an electrochemical study of synthetic analogues and Mössbauer spectroscopy, which inspired the name of the new mineral.

Unlike fougèrite and trébeurdenite, which are blue-green, pure synthetic mössbauerite is orange in colour. Detailed optical and other physical properties could not be determined because of the small platelet size and instability. The hardness is probably 2–3, by analogy with other members of the supergroup and the density, calculated from unit-cell parameters, is 2.950 g/cm^3. Synchrotron X-ray data indicate that the natural material is a nanoscale intergrowth of $2T$ and $3T$ polytypes; the latter probably has the $3T_7$ stacking sequence. The corresponding maximum possible space group symmetries are $P\bar{3}m1$ and $P3m1$. Unit-cell parameters for the $3T$ cell are a = 3.032(7) Å, c = 22.258(4) = 3 × 7.420 Å and Z = ½.

Mössbauer spectroscopy at 78 K indicates that two distinct Fe^{3+} environments exist in a 2:1 ratio. These are interpreted to be ordered within each layer, but without the development of a three-dimensional superlattice. Mössbauerite undergoes gradual magnetic ordering at 70–80 K to a

---

* E-mails: jean-marie.genin@univ-lorraine.fr; smills@museum.vic.gov.au
DOI: 10.1180/minmag.2014.078.2.14

This paper is published as part of a special issue of *Mineralogical Magazine*, Volume **78(2)**, 2014, in celebration of the International Year of Crystallography.

ferromagnetic state, below which it splits into three sextets S_{1m}, S_{2m} and S_{3m}, as measured at 15 K, and shows the same intensity ratio ½:⅙:⅓ as the three doublets for fougèrite D_{1f}, D_{2f}, D_{3f} in the paramagnetic state at 78 K. This suggests that there is also short-range coupling of interlayer carbonate anions with respect to the octahedral layers and that the 2D long-range order of carbonates in interlayers remains unchanged.

KEYWORDS: gleysols, layered double hydroxides, hydrotalcite supergroup, fougèrite, trébeurdenite, mössbauerite, polytypes, Mössbauer spectroscopy.

Introduction

THE oxidation of steels and other Fe-based materials is of major economic concern as ~5% of these materials must be replaced every year due to corrosion (Pourbaix, 1975). Girard and Chaudron (1935) noted the existence of a greenish compound on the surface of an Fe sample resting in a solution of sulfate in France and described it as "hydrolyzed magnetite". Later, in Switzerland, Feitknecht and Keller (1950) investigated Fe weathering in chlorinated media and discovered what they called "chlorinated green rust". Bernal *et al*. (1959) made the first X-ray diffraction (XRD) patterns of such compounds, determined their point-group symmetry and established their crystal structure as being of the "layered double hydroxide" (LDH) type. LDH structures consist of brucite-like layers $[(M^{2+}_{(1-x)}M^{3+}{}_x)(OH)_2]^{x+}$, carrying a net positive charge due to the partial substitution of trivalent octahedral cations for divalent cations. This charge is balanced by anions intercalated between the brucite-like layers. Water molecules may also occur in the interlayers. Over 40 naturally occurring LDH minerals have recently been classified as forming the hydrotalcite supergroup, named after the archetypal species hydrotalcite, $Mg^{2+}_6Al^{3+}_2(OH)_{16}[CO_3]\cdot4H_2O$ (Mills *et al.*, 2012*a*).

The fougèrite group minerals are the only members of the hydrotalcite supergroup in which divalent and trivalent cations belong to the same element, Fe that confers distinctive redox properties. Thus, this group represents naturally occurring green rust phases. Evidence, largely from Mössbauer spectroscopy, was reviewed by Mills *et al.* (2012*a*) who found that the Fe^{2+}:Fe^{3+} ratio does not vary continuously in the fougèrite group but that three distinct fixed-composition phases exist. The species fougèrite was redefined to correspond to the most reduced of these, $Fe^{2+}_4Fe^{3+}_2(OH)_{12}[CO_3]\cdot3H_2O$, a new name trébeurdenite was defined to correspond to $Fe^{2+}_2Fe^{3+}_4O_2(OH)_{10}[CO_3]\cdot3H_2O$, found intimately mixed with fougèrite and formerly considered to constitute part of the fougèrite solid-solution range and the discovery was announced of a new, fully oxidized mineral mössbauerite, $Fe^{3+}_6O_4(OH)_8[CO_3]\cdot3H_2O$.

The mineral mössbauerite is named after Professor Rudolf Ludwig Mössbauer (1928–2011) who discovered the resonance of γ rays that bears his name, for which he was awarded the 1961 Nobel Prize in physics. Without this technique, the very existence of this mineral in gleysols and the true nature of the 'green rust' compounds could not be understood. The mineral and name (IMA2012–049) were approved by the International Mineralogical Association (IMA) Commission on New Minerals, Nomenclature and Classification (CNMNC) prior to publication. One wet holotype sample sealed in a glass jar is preserved in the collections of Museum Victoria (Melbourne, Australia), registration number M52078. Other samples are now hosted in the Mineralogical Museum of Eötvös University (Budapest), the Mineralogical Collection of the École des Mines (Paris) and the Collection of the Université Catholique de Louvain-la Neuve (Belgium).

Oxidation mechanisms and structural characteristics of 'green rust': background

The first Mössbauer spectra for 'green rusts' were obtained by Gancedo *et al.* (1976). They clearly showed two quadrupole doublets, one with a large quadrupole splitting attributed to Fe^{2+} and a second with a small splitting attributed to Fe^{3+}, which proved that 'green rusts' contained Fe in both oxidation states. The major advantages of Mössbauer spectroscopy as a technique are that (1) the areas under the doublets are directly proportional to the relative abundance of the corresponding Fe local environments within the solid phase, allowing us to easily measure the ferric ion ratio $x = \{[Fe^{3+}]/[Fe_{total}]\}$, (2) this method is, in effect, element-specific for Fe, which avoids interference from other components in a complex phase and (3) minimal sample preparation is required, important when dealing with reactive, air-sensitive phases. In the early 1980s, Mössbauer spectroscopy became a favoured means of investigation for following the oxidation of Fe, which allowed plotting of E_h−pH (Pourbaix) diagrams demonstrating that ‘green rust’ phases were stable corrosion products of steels in appropriate aqueous media (chlorinated, sulfated, carbonated, etc: cf. Drissi *et al*., 1995; Olowe and Génin, 1991; Génin *et al*., 1996, 1998*b*, 2006*b*).

‘Gley’ in waterlogged soils was first defined over a century ago by the Ukrainian scientist Vysostskii (1905). In the 1930s, it was suggested that the bluish-green colour of gleys probably originated from an Fe^{2+}-containing mineral formed in anoxic conditions, which was tentatively suggested to be ‘ferroso-ferric hydroxide’ with formula $Fe^{2+}_{(1-x)}Fe^{3+}_x(OH)_{(2+x)}$. Although this formula is still often found in books, it was never proved that such a compound actually existed and while $Fe(OH)_2$ is well documented (and occurs in nature as the mineral amakinite), no simple ferric hydroxide corresponding to the fully oxidized endmember has ever been synthesized. In contrast, R.M. Taylor suggested that the mineral responsible for the colour of gleysol could be a ‘green rust’ (Taylor, 1980), but was never able to prove this experimentally. In 1996, a sample of gley was obtained from a perched aquifer in the forest of Fougères (Brittany). The Mössbauer spectrum of this material was obviously that of ‘green rust’ (Génin *et al*., 1998*a*, 2006*a*; Trolard *et al*., 2007). However, the species of ‘green rust’ involved remained unknown, since spectra were resolved into only two doublets, one ferric and one ferrous and at that time a discrepancy existed between the spectrum of the natural sample and that of ‘green rust’ prepared in the laboratory. The value of x for the mineral lay in a range around ½ and never exceeded ⅔, whereas the synthetic ‘green rusts’ had x restricted to the [¼−⅓] range. The interlayer anion in the mineral was thus uncertain and for a while, we did not exclude the possibility of a ‘green rust’ incorporating interlayer OH^- ions, chemically equivalent to the $Fe(OH)_{(2+x)}$ originally hypothesized. However, by 1999, there was convincing evidence that the natural sample was a carbonate, since Ona-Nguema in his thesis work succeeded in producing ‘carbonated green rust’ by bacterial reduction of ferric oxyhydroxide (lepidocrocite) using dissimilatory reducing *Shewanella putrefaciens* bacteria, in anoxic conditions that strongly resemble the natural conditions under the water table (Ona-Nguema *et al*., 2002). The crystal morphology of the bacterial product was similar to that obtained by coprecipitation at x = ⅓, but the crystal size was larger and XRD patterns gave parameters corresponding to ‘carbonated green rust’, but the Fe oxidation ratio, x, varied within the [⅓−⅔] range, as it does in nature. At first the discrepancy between the varying x value and the constant x value obtained in abiotic syntheses was not understood. First, a new mineral proposal under the name “fougèrite” was submitted, described as having the structure of a ‘green rust’ but with x varying in the [⅓−⅔] range (IMA2003−057; Trolard *et al*., 2007).

A few years later, the unusual redox behaviour exhibited by synthetic ‘green rust’ when oxidizing it with hydrogen peroxide instead of O was discovered (Génin *et al*., 2006*b*,*c*). The same behaviour appears to occur for all interlayer anions, but this study was focused on carbonate ‘green rusts’ as these are known in nature. Two different oxidation mechanisms could operate, as revealed by the time dependence of the electrode potential E_h and the pH of the solution containing the ‘green rust’: (1) oxidation by dissolution of the ‘green rust’ and precipitation of a ferric oxyhydroxide, ferrihydrite (Drissi *et al*., 1995; Benali *et al*., 2001) and (2) *in situ* oxidation by deprotonation of OH^- ions, without destruction of the ‘green rust’ crystals (Génin *et al*., 2005, 2006*b*,*c*; Ruby *et al*., 2010). The first mechanism, in which the CO_3^{2-} anions return into solution, was usually observed. This process destroys the ‘green rust’ layer on an Fe or steel surface and hence is responsible for the corrosion properties of these materials. The domain of existence of ‘green rust’ in the E_h−pH diagram has a triangular shape that coincides with the window between the domains of immunity and passivation of Fe, demonstrated empirically by corrosion scientists (cf. Pourbaix, 1975; Drissi *et al*., 1995). Oxidation *via* dissolution−precipitation is characterized by two plateaux in the E_h−time curve and the kinetics is rather slow. In contrast, the second mechanism displays a continuous increase of E_h plotted against time and much faster kinetics. Crystal morphology remains unchanged with oxidation, while the colour shifts from green to orange (Génin *et al*., 2005, 2006*b*,*c*; Ruby *et al*., 2010). The ‘green rust’ layer covering a steel substrate remains intact and the metal is passivated; this provides the resistance to weathering characteristic of steels often designated by the commercial name Cor-Ten®. The redox activity of 'green rust' minerals also leads to a new application in the environmentally benign denitrification of groundwater (Génin, 2013).

The crystal structures of 'green rust' with a wide range of interlayer anions (Cl^-, F^-, CO_3^{2-}, SO_4^{2-}, $COOH^-$, $C_2O_4^-$, SeO_4^{2-}...) as determined by XRD was found to be that of hydrotalcite (Génin and Ruby, 2004, 2008*a*,*b*), in the $3R_1$ polytype of Bookin and Drits (1993) and Mills *et al.* (2012*a*). The absence of diffraction from a supercell in the *xy* plane ($a \approx 3$ Å) indicated that the 3-layer repeat arises from offsets of hydroxide sublayers across the interlayers, rather than from 3D long-range order of interlayer species, as in some other members of the hydrotalcite supergroup (Mills *et al.*, 2012*a*). Thus, the 'green rust' phases are in general deduced to be isostructural with the $3R_1$ polytype of hydrotalcite, pyroaurite and stichtite. However, Mössbauer spectroscopy demonstrated incipient superstructure formation in that it showed a reduced diversity of local environments, consistent with two-dimensional long-range order of Fe^{2+} and Fe^{3+} ions within the cation layers, as well as some degree of registration between octahedral cations and interlayer anions (Génin and Ruby, 2004, 2008*a*,*b*). It will be seen below that XRD data indicate that layer stacking and local environments are different in mössbauerite than in typical members of the hydrotalcite supergroup.

Progressive *in situ* deprotonation of carbonate 'green rust' by addition of H_2O_2 was accompanied by the evolution of the Mössbauer spectra, with depletion of the Fe^{2+} quadrupole doublets and growth of a new Fe^{3+} doublet at 78 K. Study of the magnetic behaviour further supported the idea that two-dimensional long-range order of Fe^{2+} and Fe^{3+} occurs within brucite layers for the specific compositions x = ⅓, ⅔ and 1 (Rusch *et al.*, 2008*a*,*b*). Hence, for carbonate 'green rusts' at least, the general formula, $Fe^{2+}_{6(1-x)}Fe^{3+}_{6x}O_{12}H_{2(7-3x)}CO_3 \cdot 3H_2O$ is not represented by a continuous solid solution, but as mechanical mixtures (topotactic intergrowths) of three-line phases of those compositions with distinctive magnetic properties. The compound with x = ⅓ is the original ferrous ferric hydroxycarbonate 'green rust' $Fe^{2+}_4Fe^{3+}_2(OH)_{12}CO_3 \cdot 3H_2O$; the compound with x = ⅔ is $Fe^{2+}_2Fe^{3+}_4O_2(OH)_{10}CO_3 \cdot 3H_2O$; and that with $x = 1$, the fully oxidized formula, becomes $Fe^{3+}_6O_4(OH)_8CO_3 \cdot 3H_2O$; the latter was originally termed "ferric green rust", despite its orange colour (Génin *et al.*, 2005). A fully reduced composition with $x = 0$ would be $Fe^{2+}_6(OH)_{10}(H_2O)_2CO_3 \cdot 3H_2O$. This has not been synthesized directly by precipitation or found in nature to date, but has been obtained by voltammetric cycling of the other compounds (Legrand *et al.*, 2001).

The 'green rust' minerals found initially in gleys were from continental aquifers and had x in the [⅓–⅔] range. In 2010, it was found that gleys from coastal salt marshes were more oxidized, with x in the [⅔–1] range, probably due to their periodic exposure to air at low tide. The expanded known composition range for natural 'green rusts' and knowledge of the existence of the line phases led us to redefine fougèrite as the ordered compound at x = ⅓ and to give to the mineral with x = ⅔ the new name trébeurdenite, after the town in Brittany from where the salt-marsh gley was first extracted for study (Mills *et al.*, 2012*a*; Génin *et al.*, 2012). Mössbauerite is the completely ferric compound with $x = 1$. According to the new nomenclature (Mills *et al.* 2012*a*), natural samples extracted from continental aquifers to date are now mixtures of fougèrite and trébeurdenite, whereas those extracted from intertidal salt marshes are mixtures of trébeurdenite and mössbauerite. Note that fougèrite has also been confirmed as an alteration product from the Dronino meteorite, Ryazanskaya Oblast, Kasimov district, Russia (Igor Pekov and Nikita Chukanov data; Museum Victoria specimen M52552), which is the first occurrence of a fougèrite-group mineral outside of a waterlogged environment.

Occurrences, locations and physical properties

Mössbauerite is a secondary nanocrystalline mineral that is the product of *in situ* oxidation and deprotonation when the other minerals of the fougèrite group within a gley are exposed to air in intertidal environments; it is found in a number of maritime marsh deposits around Mont Saint-Michel Bay, in Brittany and Normandy, France (Fig. 1). Mössbauerite has also been recorded in the maritime marshes around Trébeurden, Locquirec and Paimpol (Brittany). In all the examples so far observed, mössbauerite is found as an intimate intergrowth with trébeurdenite, $Fe^{2+}_2Fe^{3+}_4O_2(OH)_{10}CO_3 \cdot 3H_2O$ and mössbauerite

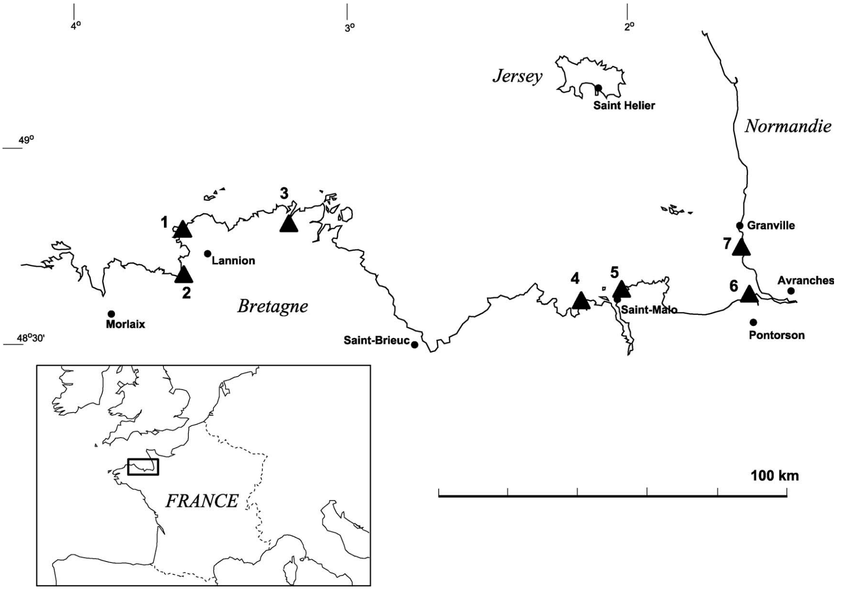

FIG. 1. Trébeurdenite–mössbauerite localities in Brittany and Normandy, northern France: (1) Penvern-Trébeurden; (2) Trédrez-Locquémeau; (3) Plougrescant; (4) Lancieux; (5) Saint-Malo; (6) Mont Saint-Michel Bay, near Mont Saint-Michel; (7) Mont Saint-Michel Bay, between Avranches and Granville.

makes up only 16–31% of the total (as observed from Mössbauer data; see below). Furthermore, these minerals are, in turn, a minor constituent (~5% by mass) of a sediment (gley) dominated by quartz, feldspars and clay minerals. The massive green-grey ‘clay-like’ gley deposits which host mössbauerite + trébeurdenite are up to several metres thick and can be found over most of the area of Mont Saint-Michel Bay and rias in Brittany (Fig. 2).

After continued exposure to air for a few hours, both trébeurdenite and mössbauerite lose H_2O and CO_2 and oxidize further to poorly crystalline Fe oxyhydroxides. It is important to note that mössbauerite has not yet been recorded in fougèrite–trébeurdenite mixtures that have remained protected from atmospheric O below the water table (e.g. those found in the Fougères forest and other continental aquifers). However, it can easily be confused with other ferric oxyhydroxides such as ferrihydrite. The precursor trébeurdenite is interpreted as having formed from bacterially mediated reduction of Fe^{3+}

FIG. 2. Preserved gleysols in marine marshes in Mont Saint-Michel Bay, France. The gley contains trébeurdenite intergrown intimately with mössbauerite.

oxyhydroxides, with concomitant oxidation of organic matter to carbonate (Ona-Nguema *et al.*, 2002).

Mössbauerite has not been identified visually in natural materials. However, individual crystallites in pure synthetic material are <0.2 µm wide and show distinct hexagonal outlines (Fig. 3) in TEM images, where the forms $\{0001\}$, $\{10\bar{1}0\}$ or $\{11\bar{2}0\}$ can be discerned. Pure synthetic material is orange in colour; natural material is mixed with green-grey (olive) trébeurdenite, which predominates. Using pure synthetic material, the following properties were obtained: crystalline aggregates have an orange streak, earthy lustre and are opaque; they are non-fluorescent in shortwave and longwave ultraviolet light and have a Mohs hardness of 2–3. The tenacity is sectile and ideally, there is one perfect cleavage direction on $\{0001\}$. The calculated density based on the formula and the unit cell of the synthetic material (a = 3.032(17) and c = 22.258(4) Å; see below) is 2.950 g/cm^3. The optical properties could not be measured due to the submicroscopic size of crystals, the mixture with trébeurdenite and the extreme reactivity of the overall material.

Chemistry and X-ray diffraction

It was not possible to analyse natural mössbauerite directly, as it is inevitably intergrown with the closely related mineral trébeurdenite as well as having nanometre-sized grains. Even separation of the combined 'green rust' minerals from other phases in the gley was not possible, given their small modal abundance, small grain size and rapid decomposition when exposed to air. Génin *et al.* (2006*a*) and Trolard *et al.* (2007) faced the same problem when analysing type fougèrite. As already noted, the minerals of the fougèrite group were first discovered by Mössbauer spectroscopy, where they are easily distinguished in the paramagnetic state at ambient or 78 K by their quadrupole doublets of two types, those with a large splitting that characterize the ferrous state and those with a small splitting that characterize the ferric state (Fig. 3 and Table 3).

Because of its instability and occurrence in fine intergrowths, detection and characterization of mössbauerite rely on techniques that can be applied to multiphase samples with minimal sample preparation, in particular, the eponymous spectroscopic method and comparison with synthetic standard materials. The type material, while wet with an excess of its associated seawater, gave an XRD peak corresponding to d_{003} of mössbauerite + trébeurdenite at an intensity implying a few % by mass of the total sample (Fig. 4). It is common for only the d_{003} of the fougèrite-group minerals to be distinguishable in XRD patterns of natural material; other lines overlap with those of the typical minerals found in

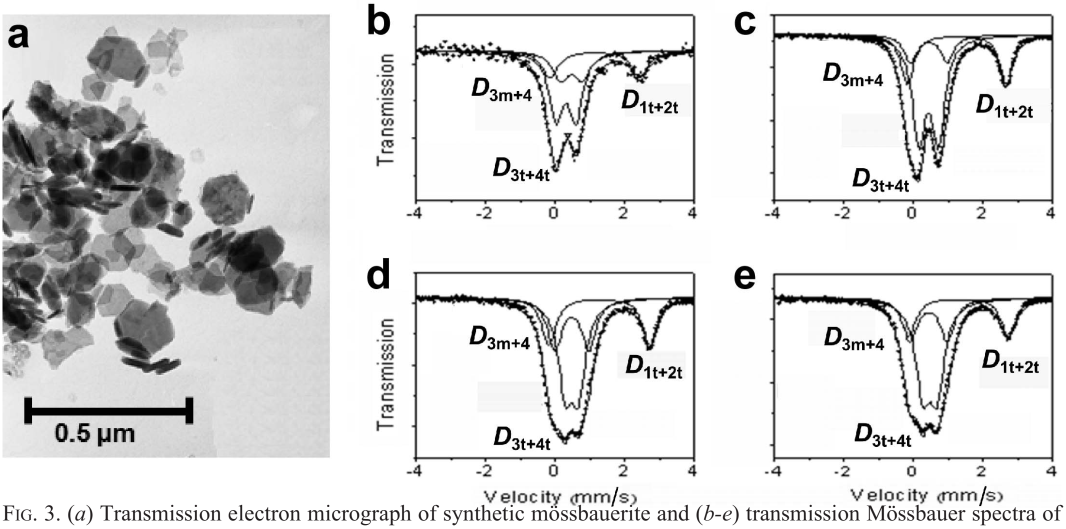

FIG. 3. (*a*) Transmission electron micrograph of synthetic mössbauerite and (*b-e*) transmission Mössbauer spectra of gley samples from Penvern-Trébeurden measured at ambient temperature and from Mont-Saint Michel Bay at 78 K (Table 3).

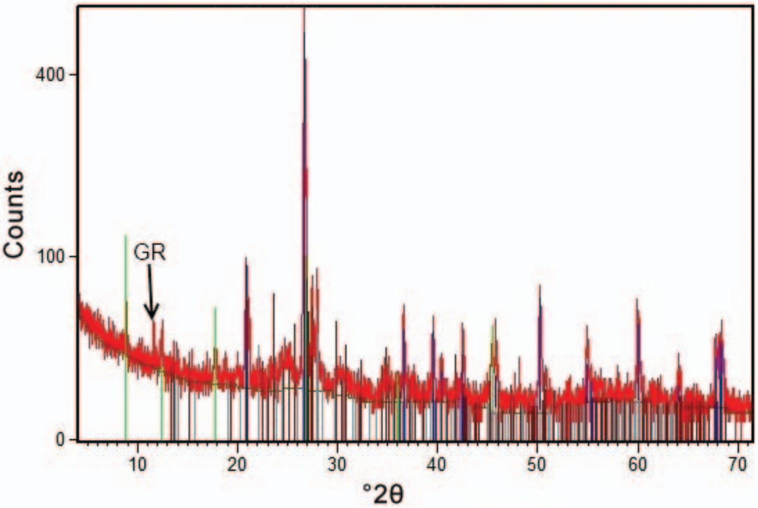

FIG. 4. Powder XRD diagram of wet gley from Mont Saint-Michel Bay (Cu$K\alpha$ radiation). Note the green rust peak which is not matched by other phases in the gley. GR = ‘green rust’ = trébeurdenite + mössbauerite. Green lines are illite, blue are quartz, brown are orthoclase and grey are albite.

gleys. In a previous study, the d_{006} was also observed (cf. Christensen *et al*., 2009). Mössbauer study proved the coexistence of the two ‘green rust’ minerals, trébeurdenite and mössbauerite (see below).

After drying the material, the diagnostic XRD peak disappeared due to decomposition of the phases (Fig. 5), which presumably lost CO_2 and H_2O and oxidized to form a poorly crystalline Fe oxyhydroxide such as ferrihydrite. This decomposition path has been shown to usually exist in synthetic samples (Drissi *et al*., 1995; Benali *et al*., 2001).

Chemical analyses of areas approximately 0.5 mm × 0.4 mm on a pressed chip of the gley X-rayed in Fig. 4 were obtained by energy-dispersive X-ray analysis using a JEOL 6400 SEM equipped with Link ISIS quantification software, at an accelerating potential of 15 kV and using 1 nA probe current at the Australian National University. Standards used were albite (Na, Al), periclase (Mg), sanidine (Si, K), apatite (P), pyrite (S, Fe), halite (Cl), diopside (Ca) and rutile (Ti). F, P and Mn were also sought but not detected.

Oxide totals obtained were only in the range 55–64% due to the porosity, surface roughness

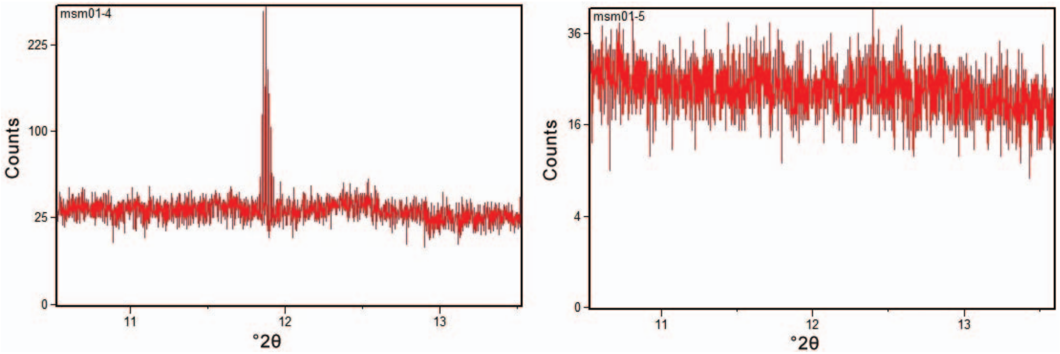

FIG. 5. ‘Green rust’ (trébeurdenite + mössbauerite) d_{003} peak in wet gley (left) and the same gley mount which had dried after several hours (right) showing no ‘green rust’. Sample from Mont Saint-Michel Bay. d_{003} = 7.449 Å.

and an unquantified but large percentage of structural water. Minor charging was observed on the sharp edges of grains, which would tend to suppress excitation of higher-energy X-rays. Hence, the measured Fe_2O_3 concentrations of 2.87, 3.72 and 4.29 wt% are considered minimum values. As Fe is not a significant component of the other phases known to be present from the XRD and also from point analyses from SEM (quartz, K-feldspar, plagioclase, illite/muscovite and kaolinite; Fig. 4), it is deduced to be present in the decomposition products of former mössbauerite + trébeurdenite; the Fe_2O_3 concentrations obtained are consistent with the modal abundances of these phases estimated from XRD.

A small quantity of Cl in the bulk analyses (0.18–0.24 wt%) is attributed to the presence of halite in the gley and does not imply the presence of a Cl-dominant ‘green rust’ mineral. Although synthetic ‘chlorinated green rust’ is known, it usually has the oxidation ratio x = ¼, sometimes reaching ⅓; this is less than that found for intertidal ‘carbonate green rust’ and hence would require much more reducing conditions (Refait and Génin, 1993). Similarly, the presence of ‘sulfated green rust’ is eliminated, as this material, also known as a synthetic phase, has a much larger layer spacing of 11.01 Å (Olowe and Génin, 1991; Simon *et al.*, 2003), which was never observed in the XRD pattern of the gley. ‘Green rust’ with interlayer CO_3^{2-} is often shown to be more stable than with SO_4^{2-}, which in turn is more stable than with Cl^- (Refait and Génin, 1994).

The ideal formula for endmember mössbauerite is $Fe_6^{3+}O_4(OH)_8CO_3{\cdot}3H_2O$, which requires Fe_2O_3 73.79, CO_2 6.78, H_2O 19.43, total 100 wt.%.

Crystal structure

Mössbauerite is known to be a layered double hydroxide (LDH) mineral, with a structure in which Fe^{3+} cations in the centre of octahedra with (OH^- and O^{2-}) anions lying at vertices share edges to form a stacking of brucite-like layers with a net positive charge, with carbonate and water in the interlayers. Initial powder XRD data collected from pure synthetic material using Cu*K*α radiation at Museum Victoria showed only six peaks, consistent with a three-layer polytype. Subsequently, a high-resolution powder diffraction pattern at low scattering angles was obtained using synchrotron X-rays at the Swiss Light Source, Paul Scherrer Institut, Zürich. Finely crushed synthetic mössbauerite was introduced in a 1 mm glass capillary. After checking the sample quality with a standard powder X-ray diffractometer using Mo*K*α_1 radiation, a high-resolution pattern was collected using monochromated X-rays of λ = 0.350156 Å and an acquisition time of 2 h. Patterns were recorded in continuous scanning mode over the 2θ range 0°–52° (Fig. 6). The wavelength was selected with a double-crystal Si(111) monochromator and refined using NIST Si powder (a = 5.43094 Å) as an internal standard, from the position of the first 10 Si reflections. The lowest-angle and strongest peaks detected included one at 7.42 Å corresponding to the LDH layer spacing, one at 22.2 Å (3 × 7.4 Å) corresponding to a three-layer polytype and one in between at 14.1 Å, corresponding approximately to a two-layer periodicity. The 14 Å and 22 Å peaks are connected by a region of intense diffuse scattering, implying considerable stacking

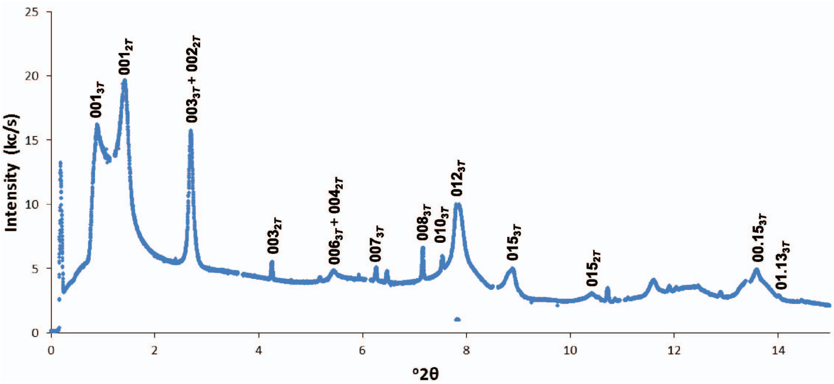

FIG. 6. Synchrotron powder XRD pattern of pure synthetic mössbauerite (λ = 0.350156 Å). Note that 001 peaks from 3*T* and 2*T* structures are connected by strong diffuse intensity, implying nanoscale intergrowths.

disorder, with intergrowths of two- and three-layer structures on the nanometric scale. Note that these peaks would index as 001 for their respective polytypes, which cannot be the highly symmetrical $3R_1$, $3R_2$, $2H_1$ or $2H_2$ structures of table 1 in Mills *et al.* (2012*a*), as the 001 reflection is systematically absent in all these cases. The two-layer structure, by elimination, must be $2T$ with highest possible space group $P\bar{3}m1$, while the three-layer structure is one of seven $3T$ possibilities with space group $P\bar{3}m1$ or $P3m1$. Hence, mössbauerite shows structural differences from fougèrite, trébeurdenite and the hydrotalcite group *sensu stricto*. Note that Richardson (2013) cast doubt on the existence of mössbauerite as a distinct phase, given that only one peak in the diffraction patterns of Mills *et al.* (2012*a*) fig. 10*b* could be attributed unambiguously to a LDH phase rather than to admixed feroxyhyte. However, observation of the strong 001 reflections from two unusual LDH polytypes in the synchrotron XRD data confirms that the synthetic sample, known to have oxidation ratio $x = 1$, consists largely of material with LDH structure type, namely mössbauerite.

Peaks observed in the synchrotron XRD pattern are listed in Table 1. Unit-cell parameters refined from the powder data for the three-layer structure using *Checkcell* (Laugier and Bochu, 2000) are $a = 3.032(17)$ Å, $c = 22.258(4) = 3 \times 7.420$ Å and $V = 177.17$ Å^3, with $Z = ½$. It was not possible to refine the two-layer cell separately, due to extensive overlap of peaks, but it is presumed to have a very similar a parameter. The 001 peak is not at the position expected for $c = 14.84 = 2 \times 7.420$ Å, but is displaced to a higher angle, implying a narrower layer spacing, $c = 14.11 = 2 \times 7.055$ Å. These data are broadly consistent with those of Ruby *et al.* (2010) for less oxidized fougèrite-group members, although the significant reduction in size of the mössbauerite unit cell reflects not only reduction in interatomic distances as a function of oxidation of Fe, but also a change in interlayer configuration, as discussed below. The unit-cell parameters for fougèrite and trébeurdenite are $a = 3.182$ Å and $c = 22.896 = 3 \times 7.632$ Å and $a = 3.173$ Å and $c = 22.695 = 3 \times 7.565$ Å, respectively (Ruby *et al.*, 2010; Mills *et al.*, 2012*a*).

Given the likelihood of preferred orientation and the small number of peaks observed, the XRD intensity information is sufficiently reliable to distinguish polytypes of the same periodicity, as used by Bookin and Drits (1993). However, it is

TABLE 1. X-ray powder diffraction data for synthetic mössbauerite. 2θ values are for $\lambda = 0.350156$ Å. The calculated d spacings based on unit-cell refinement are for the $3T$ phase only. Peaks at 5.172°, 6.475° and others unlisted in the 10−13° range cannot be assigned to either structure and are due to unknown impurities. The unlisted peak at 5.932° is very narrow and is probably a noise spike.

$2\theta_{obs}$ (°)	d_{obs} (Å)	$2\theta_{calc}$ (°)	d_{calc} (Å)	*hkl* (3*T*)	*hkl* (2*T*)	I_{obs}
0.880	22.79	0.901	22.26	001		80
1.425	14.11				001	100
2.686	7.471	2.704	7.419	003	002	65
4.256	4.715				003	1
5.172	3.880					1
5.437	3.691	5.410	3.710	006	004	2
6.251	3.211	6.313	3.180	007		3
6.475	3.099					3
7.155	2.806	7.216	2.782	008		4
7.535	2.663	7.646	2.626	010	010	4
7.854	2.557	7.857	2.555	012		30
8.874	2.263	8.880	2.261	015		13
10.404	1.930				015	1
10.860	1.850	10.833	1.855	00.12	008	2
11.108	1.809	11.108	1.809	019		<1
13.571	1.482	13.552	1.484	00.15	018	4
14.008	1.436	14.016	1.435	01.13	00.10	<1

still possible to identify the three-layer structure that is most likely to intergrow intimately with 2*T*, by consideration of the distinctive interlayer geometries of the polytypes. As in Mills *et al.* (2012*a*), the notation {*A*, *B*, *C*} is used to indicate *xy* coordinates of hydroxide sublayers and {α, β, γ} the corresponding coordinates of octahedral cations. Each (O,OH)−Fe−(O,OH) compound layer has six possible positions for the next layer, each of which creates distinguishable interlayer environments that are labelled O_{1-4}, P_{1-2} in Table 2. This nomenclature is an extension of that of Bookin and Drits (1993) and Mills *et al.* (2012*a*), where the letters '*O*' and '*P*' refer to −OH···HO− groups that are respectively offset across the interlayer, or that point at each other across the interlayer. The six local environment types are topologically distinct except for O_3 and O_4, which interconvert if the polarity of the *c* axis is reversed. All interlayers are of the same type in the high-symmetry polytypes 1*T* (O_1), $2H_1$ (P_1), $2H_2$ (O_3 or O_4), $3R_1$ (P_2) and $3R_2$ (O_2). However, this is not true for 2*T* (alternating O_2 and P_2) or for $3T_1$−$3T_7$. The sequences $3T_1$ ($O_1O_3O_3$) and $3T_4$ ($O_1P_1P_1$) have no interlayer environments in common with 2*T*. The $3T_2$, $3T_3$, $3T_5$ and $3T_6$ structures have one or the other of O_2 or P_2 represented. However, $3T_7$ ($O_1O_2P_2$) has both. This means that, in effect, the unit cell of $3T_7$ already contains that of 2*T* and stacking faults in either of these structures readily generate large domains of the other structure, surrounding the defect. Furthermore, the brucite layers are all oriented similarly in both structures, with none rotated through 180º about **c**, so the structures are readily interconverted through slip on (001). The layers are similarly oriented in the $3R_1$ structure typical of other 'green rusts', so that both 2*T* and $3T_7$ can be created easily by the slip of layers when mössbauerite is formed by oxidation of trébeurdenite. The $3T_7$ structure is the only non-rhombohedral polytype for which this is the case and hence is the most likely three-layer stacking sequence to occur in mössbauerite.

Table 2. Labels for the distinct interlayer geometries between two hydroxide layers in the layered double hydroxide structures.

Extended *O*/*P* notation	*A*β*C* layer pair
O_1	*A*β*C* - *A*β*C*
O_2	*A*β*C* - *B*γ*A*
O_3	*A*β*C* - *A*γ*B*
O_4	*A*β*C* - *B*α*C*
P_1	*A*β*C* = *C*β*A*
P_2	*A*β*C* = *C*α*B*

The unit cells of the 2*T* and $3T_7$ structures are shown in Figs 7*a* and *b*, while Fig. 7*c* shows that sporadic introduction of stacking faults can result in an aperiodic stacking sequence, which can be described as packets of $3T_7$ separated by stacking faults, or equally well as packets of 2*T* separated by stacking faults. Such a structure would produce low-angle XRD peaks very similar to those seen in our synchrotron data. The maximum-symmetry space groups for the 2*T* and $3T_7$ polytypes are $P\bar{3}m1$ and $P3m1$, respectively (Mills *et al.*, 2012*a*).

Figure 7*d* shows a portion of a brucite layer and the overlying interlayer carbonate groups, assuming that the interlayer is in the *P* configuration. The carbonates are shown in the two-dimensionally ordered pattern proposed for fougèrite by Génin *et al.* (2005). Note that this ordering pattern of carbons has six twin-related orientations and 12 choices of origin for each C in each interlayer, giving a total of 72 positional variants and that different interlayers may orient independently. It is thus unsurprising that there is no evidence of ordering in the third dimension. Carbon atoms lie either above an Fe atom of this brucite layer, or below an Fe atom of the layer above. Carbonate oxygens lie nearly above the OH groups of the brucite layer, but are slightly offset given that the C−O distance (1.29 Å) is shorter than $a/\sqrt{3}$ (1.75 Å). OH groups that do not have an overlying carbonate O have an H_2O molecule instead (not shown in the figure), also slightly displaced so as to optimize its H bonding to the OH groups above and below and to other interlayer oxygens. Figure 7*e* shows that carbonate groups can order in a similar fashion in an *O*-type interlayer, although interlayer oxygens now lie above the interstices between three Fe octahedra and below similar interstices of the next brucite layer and C atoms have an Fe atom below and a brucite O above, or *vice versa*.

It is noteworthy that interlayers of types *O* and *P* have quite different spacings. As noted above, the other minerals of the fougèrite group have layer spacings of ~7.6 Å, corresponding to *P*-type interlayers typical of other hydrotalcite-like structures (Mills *et al.*, 2012*a*). In contrast, the d_{001} spacings for 3*T* and 2*T* mössbauerite imply significantly smaller mean layer spacings. The

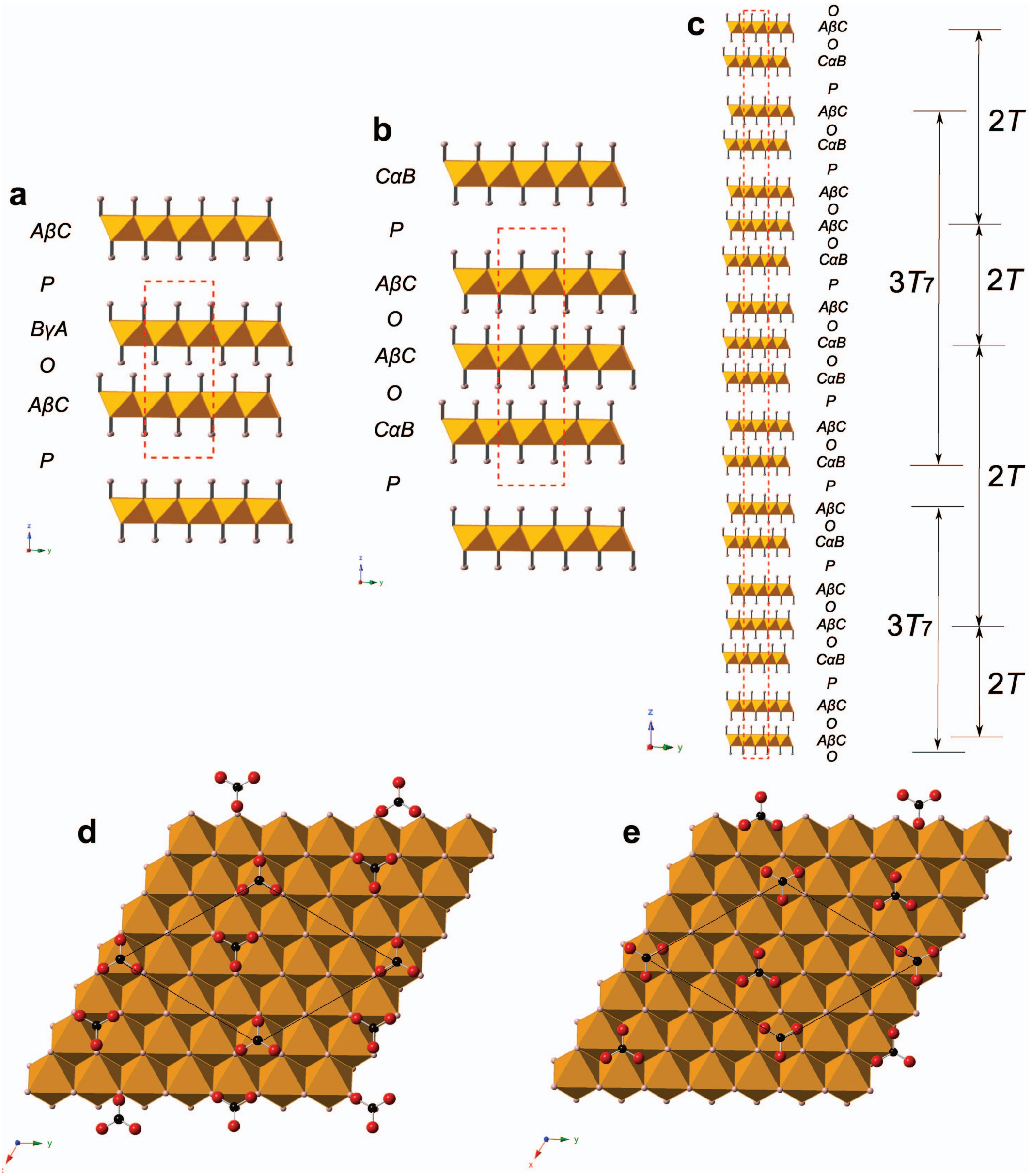

FIG. 7. The inferred crystal structure of mössbauerite. (*a*) View down *x* for 2*T* polytype, showing stacking pattern of layers of edge-sharing $Fe^{3+}(O,OH)_6$ octahedra (orange). *O* and *P* interlayer geometries are indicated, but interlayer (CO_3, H_2O) are not shown. The difference in width of the *O* and *P* interlayers is discussed in the text. (*b*) Analogous view of the $3T_7$ polytype. (*c*) Partially disordered stacking of mössbauerite layers, producing an aperiodic structure that can be described equally well as either packets of $3T_7$ separated by stacking faults, or packets of 2*T* with stacking faults. (*d*) View down **z** of one brucite-like layer assuming that the overlying interlayer is of *P* geometry. Interlayer CO_3^{2-} anions (C = black spheres, O = red) are shown ordered according to the scheme of Génin *et al*. (2005). Small pink spheres are partially occupied H of OH^-; Any H that do not have an overlying carbonate O are overlain by a water molecule (not shown). $\sqrt{12} \times \sqrt{12}$ mesh of two-dimensional ordering pattern is shown dashed. (*e*) Corresponding view for an interlayer of *O* geometry, showing that a similar carbonate ordering scheme is possible, but with CO_3^{2-} groups shifted so that oxygens do not juxtapose over the anions of the brucite sheet.

contraction is consistent with the idea that a proportion of interlayers in mössbauerite are of *O* type, which would be expected to be narrower than *P*-type interlayers.

The breadth of the peaks in Fig. 6 prevents an accurate estimation of layer spacings from the diffraction, although some constraints can be obtained from consideration of bonding geometry. The mean bond distance for Fe^{3+} octahedrally coordinated by O is expected to be 2.015 Å, from the bond-valence parameters of Brese and O'Keeffe (1991). The bond vectors have a horizontal component of $a/\sqrt{3}$ = 1.751 Å and hence a vertical component of 0.998 $\approx$ 1.0 Å. Suppose layers are stacked in a *P* configuration $A\beta C = C\alpha B$. The interlayer water molecules and carbonate oxygens will be nearly in *C* positions (slightly offset in reality, due to the short C–O bond and optimization of H bonding), while the C atoms will be in *A* or *B* positions. In this case, the interlayer spacing between the Fe layers at β and α is given by $p+q+r+r+q+p = 2(p+q+r)$, where p = half the height of the FeO_6 octahedron, estimated above as 1.0 Å, q = height of an O–H bond, also $\approx$ 1.00 Å and r = vertical component of a H bond between the H of the brucite layer and the O of an interlayer carbonate group or water molecule (differentiated below as O′), which is offset only slightly from the *C* position between the two opposed OH groups of the brucite layers: $O{-}H\cdots O'\cdots H{-}O$. The distance r will vary depending on the exact pattern of H bonding and the lateral offset of O', but ~1.8 Å would be typical, giving a total layer spacing of 7.6 Å, as observed for other members of the fougèrite group.

If layers stack in an *O* configuration such as $A\beta C{-}A\beta C$, then interlayer anions O' will lie in *B* positions and C atoms in *A* or *C*. This arrangement keeps H and O′ too far apart for strong $O{-}H\cdots O'$ hydrogen bonds, unless the interlayer gap shrinks so that H and O′ are almost coplanar. The main control on layer spacing is then the distance between O of the brucite layer and O' of the interlayer, which is unlikely to be less than ~2.8 Å, a typical minimum non-bonded distance for oxygens that do not share a strongly bound cation. The minimum vertical height ($q+r$) between O and O' then becomes ~2.2 Å and the interlayer spacing ~6.4 Å.

The estimates derived here for *O* and *P* layer spacings predict *c* repeats of ~14.0 Å and 20.6 Å for the $2T$ and $3T_7$ polytypes, respectively. The former value agrees well with the observed position of the d_{001} peak (14.1 Å), while the latter is shorter than the refined *c* parameter (22.2 Å) by ~9%. There is currently insufficient data to explain the discrepancy. A repeating *OPP* pattern of interlayers rather than *OOP* would have an expected *d* spacing of 21.6 Å, closer to that observed. However, for uniformly oriented brucite layers, regular repetition of such an interlayer pattern would not produce a $3T$ polytype but one of two possible $9R$ stacking sequences. Neither of these can account for the unindexed 3.880 and 3.099 Å peaks in Table 1 and there are no other unambiguous signs of their presence in diffraction.

Note that an interlayer C of an *O* layer must have an Fe atom vertically below it and a brucite-layer *O* vertically above it, or *vice versa*. The non-bonded $C\cdots O$ distance of $\geqslant$2.2 Å is acceptable, but there is no room for a H to be bonded to the O. Thus, the locations of the O^{2-} anions in the brucite layers must be at least partially coupled to the positions of the carbons in the interlayer and it is only possible for the interlayer to be in the *O* configuration if some hydrogens are missing from the brucite layer.

A mixed $2T{-}3T_7$ structure is unusual for a hydrotalcite-supergroup mineral in that it necessarily has >50% of the interlayers in the *O*-type configuration. Hydrotalcite itself and the vast majority of the supergroup, including the other known 'green rust' phases, have *P*-type interlayers. Polytypes with the *O* configuration (mainly $1T$ or $3R_2$) are adopted by the brucite group with no intercalated interlayer species, the wermlandite group with expanded interlayers containing large cations, some members of the woodwardite and glaucocerinite groups with interlayer SO_4^{2-}, omsite and a small number of other examples (e.g., Bookin *et al*., 1993*a*,*b*; Mills *et al*., 2011, 2012*a*,*b*). Mössbauerite is a rare exception to the rule that the *P* configuration is preferred when carbonate is present in the interlayer space. The difference in stacking compared to fougèrite and trébeurdenite is supported by the observation that sharp spots in the electron diffraction patterns of the precursor phases are replaced by arcs and spotty rings in mössbauerite (Génin *et al*., 2006*c*; Mills *et al*., 2012*a*). This implies that although solid-state transformation from the precursor phases does not significantly change the hexagonal morphology of the platelets, disruption of the stacking including wholesale rotation of layer packets does occur during transformation. As implied above, the high proportion of oxide anions in the 'hydroxide' layers of mössbauerite is necessary for adoption of the *O* configuration and may actively stabilize the change in stacking preference. Further, the large proportion of *O* layers increases the resemblance of mössbauerite stacking to that in the metastable FeO(OH) polymorph feroxyhyte (Carlson and Schwertmann, 1980), which is isostructural with brucite and is a potential decarbonation and dehydration product of mössbauerite.

Mössbauer spectroscopy

The separate identities of the minerals mössbauerite, trébeurdenite and fougèrite have been established by a careful study of synthetic samples for comparing Mössbauer spectra of natural materials with those of synthetic reference samples. All three species are members of the hydrotalcite supergroup, of general formula $Fe^{2+}_{6(1-x)}Fe^{3+}_{6x}O_{2(3x-1)}(OH)_{2(7-3x)}CO_3 \cdot 3H_2O$, where x is the molar ion ratio $\{[Fe^{3+}]/([Fe^{2+}]+[Fe^{3+}])\}$ (Génin *et al.*, 2012). The complex history of characterization and differentiation of these phases is reviewed in the hydrotalcite supergroup nomenclature report (Mills *et al.*, 2012*a*) and references cited therein. It is possible to synthesize material with any value of x in the range [⅓–1], but the variation of x with electrode potential E_h implies that such a material is in fact a mechanical mixture of either two fixed-composition phases with x = ⅓ and x = ⅔ respectively, or of two phases with x = ⅔ and x = 1 (Génin *et al.*, 2006*c*).

Low-temperature Mössbauer spectra show distinctive magnetic ordering behaviour of Fe^{2+} and Fe^{3+} electron spins within individual sublayers for the different phases (Rusch *et al.* 2008*a*,*b*). The data for x = ⅓ show that Fe^{2+} and Fe^{3+} form distinct magnetic sublattices. Each orders ferromagnetically within a given brucite layer, but the two substructures undergo antiparallel magnetic coupling, producing ferrimagnetic behaviour with Néel temperature of ~5 K. Conversely, the x = 1 phase is ferromagnetic with a Curie temperature near 80 K and a broad superparamagnetic range of transition, while the x = ⅔ phase shows similar ferromagnetic ordering of Fe^{3+}, combined with a signal from small domains of Fe^{2+} that remains paramagnetic down to 4.2 K (Rusch *et al.*, 2008*a*,*b*). The type fougèrite (Trolard *et al.*, 2007) was found to contain both x = ⅓ and x = ⅔ phases, now redefined as fougèrite and trébeurdenite, respectively, in the nomenclature report of Mills *et al.* (2012*a*). The discovery of natural occurrences of the mixture of x = ⅔ and x = 1 led to the proposal of the x = 1 phase as the new mineral mössbauerite (cf. also Mills *et al.*, 2012*a*; Génin *et al.*, 2012).

The magnetic behaviour of fougèrite implies strong two-dimensional ordering of Fe^{2+} and Fe^{3+} within a layer. For the ratio Fe^{2+}:Fe^{3+} = 2:1, the only likely ordering pattern is that in which Fe^{2+} cations form a honeycomb arrangement with Fe^{3+} at the centre of the hexagons (Fig. 8). This minimizes local charge imbalance and cation–cation repulsion by avoidance of edge-sharing between Fe^{3+} octahedra and for x = ⅓, is the only arrangement for which such avoidance is possible. Mössbauer spectra testify that there is also a coupling between interlayer species and octahedral Fe^{2+} and Fe^{3+} in fougèrite (discussed below). Low-temperature data for mössbauerite suggests that this is true for the entire group, although the details necessarily differ for the different phases (Rusch *et al.*, 2008*a*,*b*). However, the absence of XRD peaks corresponding to development of any superstructure in the *xy* plane implies that local coupling does not propagate from layer to layer in the fougèrite group, although superstructures are known for other members of the hydrotalcite supergroup (Mills *et al.*, 2012*a*).

Mössbauer spectra for a suite of synthetic reference samples evolve systematically with Fe oxidation ratio (figs 7, 8 and 12–14 of Mills *et al.*, 2012*a*). Mössbauer doublets were deconvolved using a Voigt profile (Génin *et al.*, 2006*a*,*c*; Ruby *et al.*, 2006; Génin *et al.*, 2012) and an assignment scheme was employed in which the known correlation between Mössbauer parameters and Fe oxidation state and the compositional dependences of peak intensities were used to interpret peaks in terms of local Fe cation environments. Peaks were labelled as follows (see Tables 3 and 4):

D_1: Fe^{2+}. Always three times more intense than D_2, where the two are resolved, hence corresponding to Fe^{2+} that is not in vertical registry with the central C of a CO_3^{2-} anion within interlayers (below and above), as discussed below. Absent for mössbauerite.

D_2: Fe^{2+}. Always three times less intense than D_1, where the two are resolved, hence corresponding to Fe^{2+} in vertical registry with the central C of a CO_3^{2-} anion within an interlayer, either below or above. Absent for mössbauerite.

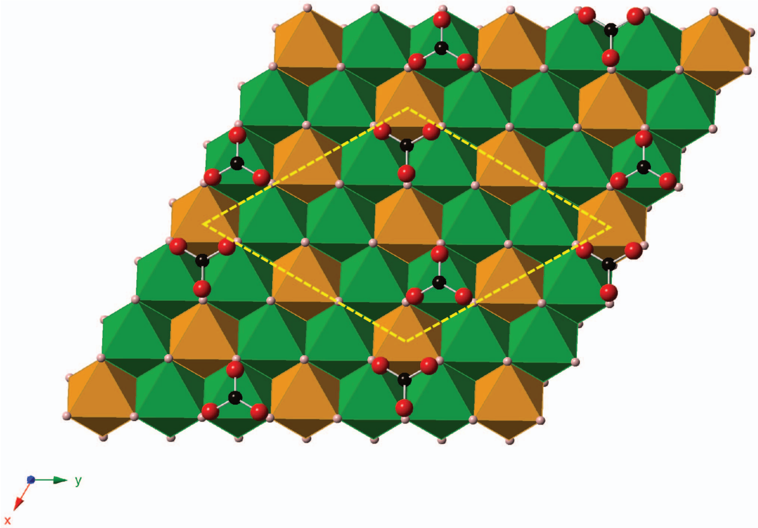

FIG. 8. The 'honeycomb' ordering pattern of Fe^{2+} (green) and Fe^{3+} (orange) proposed for the brucite layer of fougèrite. The dashed line shows a repeat of the two-dimensional $\sqrt{12} \times \sqrt{12}$ superstructure. Carbonate anions of the interlayer above are shown, ordered according to the scheme of Génin *et al.* (2005), but interlayer H_2O molecules are omitted for clarity. Six out of eight Fe^{2+} per unit mesh are in the D_1 Mössbauer environment, but the Fe^{2+} that is overlain by C is D_2, as is one other Fe^{2+} which lies over a C in the interlayer underneath (not shown). All Fe^{3+} are D_3 in fougèrite.

TABLE 3. Mössbauer parameters for Lorentzian quadrupole doublets in gley samples extracted from maritime marshes. Spectra are measured in the paramagnetic state; δ: isomer shift in mm s^{-1} (reference is α-iron at ambient temperature); Δ: fitted value of quadrupole splitting in mm s^{-1}; *RA* (%): relative area of peak doublets as a percentage of total intensity; Γ: half-width at half maximum (mm s^{-1}). T and M are trébeurdenite and mössbauerite, respectively (Fig. 3*b*–*e*).

Quadrupole doublet		$D_{1t}+D_{2t}$ Fe^{2+}(T)	$D_{3t}+D_{4t}$ Fe^{3+}(T)	$D_{3m}+D_{4m}$ Fe^{3+}(M)
Trébeurden			Room temperature	
	δ (mm s^{-1})	1.294	0.301	0.307
x = 0.75	Δ (mm s^{-1})	2.66	0.549	0.972
(75% T, 25% M)	*RA* (%)	25	50	25
	Γ (mm s^{-1})	0.56	0.45	0.49
Mont Saint-Michel Bay			78 K	
Nº1	δ (mm s^{-1})	1.245	0.429	0.441
x = 0.72	Δ (mm s^{-1})	2.842	0.560	1.059
(84% T, 16% M)	*RA* (%)	28	56	16
	Γ (mm s^{-1})	0.45	0.49	0.50
Nº2	δ (mm s^{-1})	1.263	0.471	0.470
x = 0.74	Δ (mm s^{-1})	2.908	0.381	0.986
(78% T, 22% M)	*RA* (%)	26	52	22
	Γ (mm s^{-1})	0.45	0.49	0.50
Nº3	δ (mm s^{-1})	1.292	0.466	0.434
x = 0.77	Δ (mm s^{-1})	2.877	0.405	1.073
(69% T, 31% M)	*RA* (%)	23	46	31
	Γ (mm s^{-1})	0.45	0.49	0.50

TABLE 4. Relative abundances (*RA*) of components observed in Mössbauer spectra of synthetic samples of fougèrite and mössbauerite. Measurements were taken at 78 K in the paramagnetic state, giving quadrupole doublets denoted D_n or at 4 K leading to magnetic splitting: either Zeeman splitting for ferric state to give sextuplets S_n, or mixtures of quantum states giving octets O_n. This demonstrates that Fe^{2+} sites in fougèrite are transformed into homologous Fe^{3+} sites in mössbauerite by deprotonation and demonstrating the retention of the 2D order of carbonates in interlayers from fougèrite to mössbauerite.

	Temperature	—— Fe^{2+} ——		———— Fe^{3+} ————		
Fougèrite						
paramagnetic	78 K	D_1	D_2	D_3		
RA		½	⅙	⅓		
ferrimagnetic	4 K	O_1	O_2	S_3		
RA		½	⅙	⅓		
Mössbauerite						
paramagnetic	78 K			D_3	D_4	
RA				⅓	⅔	
ferromagnetic	15 K			S_3	S_1	S_2
RA				⅓	½	⅙

D_3: Fe^{3+}. Constant in intensity at ⅓ of total for all three minerals, hence corresponding to the Fe^{3+} of fougèrite and the Fe^{3+} of the other phases that is not produced by oxidation and deprotonation processes.

D_4: Fe^{3+}. Absent in fougèrite and strongest in mössbauerite (where it is ⅔ of the total intensity). This peak replaces both D_1 and D_2 of fougèrite as the composition becomes more oxidized. Hence, D_4 corresponds to Fe^{3+} cations that are formed by oxidation of cations that were Fe^{2+} in the former fougèrite.

Whether D_4 Fe^{3+} atoms are derived from D_1 or D_2 Fe^{2+}, no further splitting at 78 K has been resolved in D_4, due to small quadrupole splitting compared to the peak widths. However, resolution of D_1- and D_2-like environments occurs below the Curie temperature of 80 K leading to sextets S_1 and S_2 (see below and Table 4). The changes in local environment that distinguish D_3 and D_4 Fe^{3+} atoms are clearly attributed to the local distributions of O^{2-} and OH^- in the brucite sheet and CO_3^{2-} and H_2O in the adjacent interlayers.

The Mössbauer doublets D_{1-4} have separate parameters for the different minerals in principle, as they have different populations of Fe^{2+} and Fe^{3+} as their nearest neighbours within the brucite sheet. Therefore, phase-specific doublets were labelled D_{1f} and D_{2f} (fougèrite) *vs*. D_{1t} and D_{2f} (trébeurdenite), D_{4t} (trébeurdenite) *vs*. D_{4m} (mössbauerite), etc. These doublets were not always fully resolved for the ferric state.

Mössbauer studies below the Néel temperature for fougèrite at 4 K display two octets O_1 and O_2, due to a mixture of quantum states for Fe^{2+} ions where the large quadrupole splitting cannot be considered as a perturbation of the Zeemann splitting and one sextet S_3 for Fe^{3+} ions; they are in the ½:⅙:⅓ intensity ratio as for the three doublets D_{1f}, D_{2f}, D_{3f} in the paramagnetic state (Rusch *et al*., 2008*a*,*b*).

Finally, Mössbauer studies below the Curie temperature for mössbauerite (~80 K) show three sextets in the ferromagnetic state at 15 K, which are in the same ½:⅙:⅓ intensity ratio as the three doublets for fougèrite D_{1f}, D_{2f}, D_{3f} in the paramagnetic state at 78 K (Rusch *et al*., 2008*a*,*b*). It is obvious that S_{1m} and S_{2m}, analogous to D_1 and D_2, represent resolution of the D_4 doublet depending on the nearby interlayer environment (whether C is in vertical registry or not).

Mössbauer parameters, doublet assignments and derived bulk Fe oxidation ratios are shown in Table 3 for the mössbauerite + trébeurdenite samples of Mills *et al*., 2012*a* (their fig. 12) and Génin *et al.* (2012). Additional Mössbauer data and analysis are also presented in these papers for mössbauerite and the other members of the fougèrite group.

Possible short-range coupling schemes

The complex Mössbauer spectrum of mössbauerite compared to that of fougèrite demonstrates that there is considerable short-range coupling in the structure, beyond the long-range average picture that can be established by XRD. Aspects of the structure that may show this short-range coupling include: (1) the polytypic stacking of brucite sheets and associated *O*/*P* geometry of the interlayer spaces; (2) alignment of interlayer CO_3^{2-} and H_2O with the Fe^{2+}/Fe^{3+} or O^{2-}/OH^- of the adjacent brucite layers; and (3) distribution of Fe^{2+}/Fe^{3+} and O^{2-}/OH^- in the brucite layers.

For the related but more reduced phase fougèrite, with no O^{2-} in the brucite layers, a short-range ordering pattern has been proposed that explains the Mössbauer data (Génin and Ruby, 2004, 2008*a*,*b*; Génin *et al.*, 2005, 2006*b*, 2012). The 'honeycomb' ordering scheme of Fig. 8 allows the Fe^{3+} of fougèrite to avoid edge-sharing with one another, while producing a highly symmetrical $\sqrt{12} \times \sqrt{12}$ superstructure in the brucite layer. The occurrence of a distinct D_2 doublet for Fe^{2+} at ⅓ of the intensity of D_1 is interpreted to correspond to Fe^{2+} which lies in close non-bonded contact with the C of an interlayer carbonate group. Note that the unit mesh of the supercell contains $6D_1$ Fe^{2+}, $2D_2$ Fe^{2+} and $4D_3$ Fe^{3+}. The corresponding part of an interlayer region contains $2CO_3^{2-}$ and $6H_2O$. If the layers are stacked in the $3R_1$ sequence with a $A\beta C = C\alpha B$ arrangement of components in a pair of adjacent layers (P_2 of Table 2), then interlayer carbonate oxygens and water molecules adopt approximate *C* positions so as to maximize H bonding. The carbons may then be in *A* or *B* positions and can align with either an α Fe^{2+} in the layer above, or a β Fe^{2+} in the layer below, respectively. In the most symmetrical case, 50% of the C atoms of each interlayer are oriented in each direction and a local short-range order pattern is obtained similar to that of Fig. 8, which accounts for the distinction between D_1 and D_2 Fe^{2+} environments. All C atoms of an interlayer are either directly above or directly below an Fe^{2+} cation, so this arrangement can be interpreted as avoidance of D_3 Fe^{3+} by C atoms. Note that the symmetry of the brucite layer in conjunction with adjacent interlayers is reduced to triclinic, so many twin-related and translationally-offset variants are possible, making it unlikely that such a pattern would undergo full three-dimensional long-range order, as discussed earlier.

Mössbauerite differs from fougèrite in that: (1) All Fe is now Fe^{3+}, ⅓ of it in an environment which is similar to that of Fe^{3+} in fougèrite (D_3 Mössbauer doublet) and the rest in a quite distinct environment that is not present in fougèrite (D_4). (2) Out of the anions in the brucite layer, ⅓ are now O^{2-}, which is not present in fougèrite. (3) The polytypic stacking of brucite layers has changed from the $3R_1$ pattern of fougèrite, very typical of the hydrotalcite group, to less regular $2T$ and $3T_7$ patterns. This implies that mössbauerite has a greater diversity of interlayer geometries; while some interlayers are of type P_2 as for the $3R_1$ polytype, others are O_1 and O_2.

These differences will clearly have an effect on the possibilities for short-range coupling in mössbauerite and also in trébeurdenite, which is compositionally halfway between mössbauerite and fougèrite and shows 'intermediate Mössbauer behaviour'. The nature of those consequences remains an area of active study.

Conclusions

Mössbauer spectroscopy has been found to be a vital technique for understanding the constitution of gleysols. Without it, the bluish-green colour of these soils would have remained unexplained. The compounds responsible for the colour were eventually found to be similar to 'green rusts', already known in connection with the corrosion of Fe and steels. However, minerals found in gleysols were more oxidized than compounds prepared previously in the laboratory. Electrochemical studies and, again, Mössbauer spectroscopy revealed that these phases show outstanding redox flexibility of 'green rusts' due to easy *in situ* deprotonation concomitant with oxidation of Fe^{2+} to Fe^{3+}. Furthermore, carbonate 'green rust' with varying overall oxidation ratio corresponded to intimate mixtures of three fixed-composition phases with $x = Fe^{3+}/(Fe^{2+}+Fe^{3+})$ = ⅓, ⅔ and 1. The formulae of these phases all correspond to $Fe^{2+}_{6-6x}Fe^{3+}_{6x}O_{4x}\ (OH)_{12-4x}(CO_3)\cdot 3H_2O$. Examples of two-phase mixtures have been found in nature, with the result that all three phases have now been defined as minerals: fougèrite (x = ⅓), trébeurdenite (x = ⅔) distinguished out of the formerly presumed fougèrite solid solution and mössbauerite (x = 1), described here. These minerals form the fougèrite group of the hydrotalcite supergroup (Mills *et al.*, 2012*a*).

While fougèrite may have the $3R_1$ polytypic structure typical of many other members of the hydrotalcite supergroup, low-angle synchrotron XRD data shows 001 peaks from two-layer and three-layer structures for mössbauerite, connected by strong diffuse intensity. Therefore, mössbauerite consists of an intimate intergrowth of at least two different polytypes, neither of them maximal-degree-of-order. The two-layer structure must be $2T$ of Mills *et al.* (2012*a*) and we argue that the $3T$ structure is the only one with all its brucite octahedral sheets similarly oriented, namely $3T_7$. Low-angle diffraction data for other members of the fougèrite group and synthetic 'green rust' phases should be examined for evidence that they too have structures with unusual stacking sequences.

Mössbauer spectroscopic data implies that there is considerable short-range coupling in the structures of the fougèrite group, which is not shown by XRD. Fougèrite itself contains two distinct environments for Fe^{2+} cations, which are interpreted as resulting from the selective close approach of interlayer C atoms to ¼ of the Fe^{2+} cations of the adjacent brucite layers. Carbon avoids D_3 Fe^{3+} in fougèrite. Spectra collected at 78 K show no splitting of the D_4 Fe^{3+} environment that progressively replaces Fe^{2+} in trébeurdenite and mössbauerite. However, there is evidence from low-temperature spectra that coupling to the interlayer C persists. The fougèrite group, including mössbauerite, are challenging to detect and characterize, as they occur in thin μm-scale plates and decompose rapidly when exposed to air. Nevertheless, they are probably very widely distributed in gleys in soil profiles. Oxidation from fougèrite through trébeurdenite to mössbauerite occurs readily by oxidation–deprotonation, while bacterial activity can regenerate reduced fougèrite (Ona-Nguema *et al.*, 2002; Ruby *et al.*, 2006). The reduced species selectively reduce groundwater nitrate to molecular N; redox activity such as this suggests that these minerals play a major role in the natural purification of aquifers (Génin, 2013).

Acknowledgements

Fernando Colombo provided helpful comments on the manuscript which improved it greatly. The authors gratefully acknowledge access to facilities at the Centre for Advanced Microscopy, ANU, funded through the Australian Microscopy and Microanalysis Research Facility. CerveauNP of the French Agence Nationale de la Recherche helped to finance part of this study.

References

Benali, O., Abdelmoula, M., Refait, Ph. and Génin, J.-M.R. (2001) Effect of orthophosphate on the oxidation products of Fe(II)-Fe(III) hydroxycarbonate: the transformation of green rust to ferrihydrite. *Geochimica et Cosmochimica Acta*, **65**, 1715–1726.

Bernal, J.D., Dasgupta, D.R. and Mackay, A.L. (1959) The oxides and hydroxides of iron and their structural inter-relationships. *Clay Minerals Bulletin*, **4**, 15–30.

Bookin, A.S. and Drits, V.A. (1993) Polytype diversity of the hydrotalcite-like minerals. I. Possible polytypes and their diffraction features. *Clays and Clay Minerals*, **41**, 551–557.

Bookin, A.S., Cherkashin, V.I. and Drits, V.A. (1993*a*) Reinterpretation of the X-ray diffraction patterns of stichtite and reevesite. *Clays and Clay Minerals*, **41**, 631–634.

Bookin, A.S., Cherkashin, V.I. and Drits, V.A. (1993*b*) Polytype diversity of the hydrotalcite-like minerals. II. Determination of the polytypes of experimentally studied varieties. *Clays and Clay Minerals*, **41**, 558–564.

Brese, N.E. and O'Keeffe, M. (1991) Bond-valence parameters for solids. *Acta Crystallographica*, **B47**, 192–197.

Carlson, L. and Schwertmann, U. (1980) Natural occurrence of feroxyhite (δ-FeOOH). *Clays and Clay Minerals*, **28**, 272–280.

Christensen, B.C., Balic-Zunic, T., Dideriksen, K. and Stipp, S.L.S. (2009) Identification of green rust in groundwater. *Environmental Science & Technology*, **43**, 3436–3441.

Drissi, S.H., Refait, Ph., Abdelmoula, M. and Génin, J.-M.R. (1995) The preparation and thermodynamic properties of Fe(II)-Fe(III) hydroxycarbonate (green rust 1); Pourbaix diagram of iron in carbonate-containing aqueous media. *Corrosion Science*, **37**, 2025–2041.

Feitknecht, W. and Keller, G. (1950) Über die Dunkelgrünen Hydroxyverbindungen des Eisens. *Zeitschrift für Anorganische und Allgemeine Chemie*, **262**, 61–68 [in German].

Gancedo, J.R., Martínez, M.L. and Oton, J.M. (1976) Mössbauer spectroscopy study of corrosion products of iron with ammonium nitrate in aqueous solutions. *Journal de Physique*, **37**, C6 297–C6 299.

Génin, J.-M.R. (2013) From fougèrite to mössbauerite through trébeurdenite; redox reactions in gleysols and role of bacteria. *Mössbauer Effect Reference and Data Journal, Chinese Academy of Sciences*, **36**, 113–160.

Génin, J.-M.R. and Ruby, C. (2004) Anion and cation distribution in Fe(II-III) hydroxysalts green rusts from XRD and Mössbauer analysis (carbonate, chloride, sulphate...); the "fougèrite" mineral. *Solid*

State Science, **6**, 705−718.

Génin, J.-M.R. and Ruby, C. (2008*a*) Composition and anion ordering in some $Fe^{II\text{-}III}$ hydroxysalt green rusts (carbonate, oxalate, methanoate); the fougèrite mineral. *Solid State Science*, **10**, 244−259.

Génin, J.-M. R. and Ruby, C. (2008*b*) Structure of some $Fe^{II\text{-}III}$ hydroxysalt green rusts (carbonate, oxalate, methanoate) from Mössbauer spectrsocopy. *Hyperfine Interactions*, **185**, 191−196.

Génin, J.-M.R., Olowe, A.A., Refait, Ph. and Simon, L. (1996) On the stoichiometry and Pourbaix diagram of Fe(II)-Fe(III) hydroxy-sulphate or sulphate-containing green rust 2: an electrochemical and Mössbauer spectroscopy study. *Corrosion Science*, **38**, 1751−1762.

Génin, J.-M.R., Bourrié, G., Trolard, F., Abdelmoula, M., Jaffrezic, A., Refait, Ph., Maitre, V., Humbert, B. and Herbillon, A. (1998*a*) Thermodynamic equilibria in aqueous suspensions of synthetic and natural Fe(II)-Fe(III) green rusts: occurrences of the mineral in hydromorphic soils. *Environmental Science & Technology*, **32**, 1058−1068.

Génin, J.-M.R., Refait, Ph., Simon, L. and Drissi, S.H. (1998*b*) Preparation and E_h-pH diagrams of Fe(II)-Fe(III) green rust compounds; hyperfine interaction characteristics and stoichiometry of hydroxy-chloride, -sulphate and -carbonate. *Hyperfine Interactions*, **111**, 313−318.

Génin, J.-M.R., Aïssa, R., Géhin, A., Abdelmoula, M., Benali, O., Ernstsen, V., Ona-Nguema, G., Upadhyay, C. and Ruby, C. (2005) Fougèrite and $Fe^{II\text{-}III}$ hydroxycarbonate green rust: ordering, deprotonation and/or cation substitution; structure of hydrotalcite-like compounds and mythosic ferrosic hydroxide $Fe(OH)_{(2+x)}$. *Solid State Sciences*, **7**, 545−572.

Génin, J.-M.R., Abdelmoula, M., Ruby, C. and Upadhyay, C. (2006*a*) Speciation of iron; characterisation and structure of green rusts and $Fe^{II\text{-}III}$ hydroxycarbonate fougèrite. *Comptes Rendus Geosciences*, **338**, 402−419.

Génin, J.-M.R., Ruby, C., Géhin, A. and Refait, Ph. (2006*b*) Synthesis of green rusts by oxidation of $Fe(OH)_2$, their products of oxidation and reduction of ferric oxyhydroxides; E_h-pH Pourbaix diagrams. *Comptes Rendus Geosciences*, **338**, 433−446.

Génin, J.-M.R., Ruby, C. and Upadhyay, C. (2006*c*) Structure and thermodynamics of ferrous, stoichiometric and ferric oxyhydroxycarbonate green rusts; redox flexibility and fougèrite mineral. *Solid State Science*, **8**, 1330−1343.

Génin, J.-M.R., Guérin, O., Herbillon, A.J., Kuzman, E., Mills, S.J., Morin, G., Ona-Nguema, G., Ruby, C. and Upadhyay, C. (2012) Redox topotactic reactions in $Fe^{II\text{-}III}$ (oxy)-hydroxycarbonate new minerals related to fougèrite in gleysols; ''trébeurdenite'' and ''mössbauerite''. *Hyperfine Interactions*, **204**, 71−81.

Girard, A. and Chaudron, G. (1935) Sur la constitution de la rouille. *Comptes Rendus de l'Academie des Sciences de Paris*, **200**, 127−129.

Laugier, J. and Bochu, B. (2000) *CHECKCELL*: a software performing automatic cell/space group determination. *Collaborative computational project number* **14** (CCP14). Laboratoire des Materiaux et du Genie Physique de l'Ecole Superieure de Physique de Grenoble, France.

Legrand, L., Abdelmoula, M., Géhin, A., Chaussé, A. and Génin, J.-M.R. (2001) Electrochemical formation of a new Fe(II)-Fe(IIII) hydroxy-carbonate green rust: characterisation and morphology. *Electrochimica Acta*, **46**, 1815−1822.

Mills, S.J., Whitfield, P.S., Wilson, S.A., Woodhouse, J.N., Dipple, G.M., Raudsepp, M. and Francis, C.A. (2011) The crystal structure of stichtite, re-examination of barbertonite, and the nature of polytytpism in MgCr hydrotalcites. *American Mineralogist*, **96**, 179−187.

Mills, S.J., Christy, A.G., Génin, J.-M.R., Kameda, T. and Colombo, F. (2012*a*) Nomenclature of the hydrotalcite supergroup: natural layered double hydroxides. *Mineralogical Magazine*, **76**, 1289−1336.

Mills, S.J., Kampf, A.R., Housley, R.M., Favreau, G., Pasero, M., Biagioni, C., Merlino, S., Berbain, C. and Orlandi, P. (2012*b*) Omsite, $(Ni,Cu)_2Fe^{3+}(OH)_6[Sb(OH)_6]$, a new member of the cualstibite group from Oms, France. *Mineralogical Magazine*, **76**, 1347−1354.

Olowe, A.A. and Génin, J.-M.R. (1991) Mechanism of oxidation of ferrous hydroxide in sulfated aqueous media: importance of the initial ratio of the reactants. *Corrosion Science*, **32**, 965−984.

Ona-Nguema, G., Abdelmoula, M., Jorand, F., Benali, O., Géhin, A., Block, J.C. and Génin, J.-M.R. (2002) Iron (II,III) hydroxycarbonate green rust formation and stabilization from lepidocrocite bioreduction. *Environmental Science & Technology*, **36**, 16−20.

Pourbaix, M. (1975) *Leçons en corrosion électrochimique*. CEBELCOR, Brussels, 377 pp.

Refait, Ph. and Génin, J.-M.R. (1993) The oxidation of ferrous hydroxide in chloride-containing aqueous media and Pourbaix diagrams of green rust one. *Corrosion Science*, **34**, 797−819.

Refait, Ph. and Génin, J.-M.R. (1994) The transformation of chloride-containing green rust one into sulphated green rust two by oxidation in mixed Cl−áand SO_4^{2-} aqueous media. *Corrosion Science*, **36**, 55−65.

Richardson, I.G. (2013) Clarification of possible ordered distributions of trivalent cations in layered double hydroxides and an explanation for the observed variation in the lower solid-solution limit. *Acta Crystallographica*, **B69**, 629−633.

Ruby, C., Upadhyay, C., Géhin, A., Ona-Nguema, G. and Génin, J.-M.R. (2006) In situ redox flexibility of Fe^{II-III} oxyhydroxycarbonate green rust and fougèrite. *Environmental Science & Technology*, **40**, 4696−4702.

Ruby, C., Abdelmoula, M., Naille, S., Renard, A., Khare, V., Ona-Nguema, G., Morin, G. and Génin, J.-M.R. (2010) Oxidation modes and thermodynamics of Fe^{II-III} oxyhydroxycarbonate green rust: dissolution-precipitation versus *in situ* deprotonation. *Geochimica et Cosmochimica Acta*, **74**, 953−966.

Rusch, B., Génin, J.-M.R., Ruby, C., Abdelmoula, M. and Bonville, P. (2008*a*) Ferrimagnetic properties in Fe^{II}-Fe^{III} (oxy)hydroxycarbonate green rusts. *Solid State Sciences*, **10**, 40−49.

Rusch, B., Génin, J.-M.R., Ruby, C., Abdelmoula, M. and Bonville, P. (2008*b*) Mössbauer study of magnetism in Fe^{II}-Fe^{III} (oxy)hydroxycarbonate green rusts; ferrimagnetism of Fe^{II}-Fe^{III} hydroxycarbonate. *Hyperfine Interactions*, **187**, 7−12.

Simon, L., François, M., Refait, Ph., Renaudin, G., Lelaurain, M. and Génin, J.-M.R. (2003) Structure of the Fe(II-III) layered double hydroxylsulphate green rust two from Rietveld analysis. *Solid State Sciences*, **5**, 327−334.

Taylor, R.M. (1980) Formation and properties of Fe(II)-Fe(III) hydroxy-carbonate and its possible significance in soil formation. *Clay Minerals*, **15**, 369−382.

Trolard, F., Bourrié, G., Abdelmoula, M., Refait, Ph. and Feder, F. (2007) Fougèrite, a new mineral of the pyroaurite-iowaite group: description and crystal structure. *Clays and Clay Minerals*, **55**, 323−334.

Vysostskii, G.N. (1905) Gley. *Eurasian Soil Science (Pochvovedenie)*, **4**, 291−327.